# Volumetric development of the zebra finch brain throughout the first 200 days of post-hatch life traced by in vivo MRI

**Original research article - Title page**

# Volumetric development of the zebra finch brain throughout the first 200 days of post-hatch life traced by *in vivo* MRI

**Author names**

Julie Hamaide [a], Geert De Groof [a], Lisbeth Van Ruijssevelt [a], Kristina Lukacova[b], Johan Van Audekerke[a], Marleen Verhoye[a], Annemie Van der Linden [a]

**Author affiliations**

[a] Bio-Imaging lab, Department of Biomedical Sciences, University of Antwerp, 2610 Antwerp, Belgium

[b] Centre of Biosciences, Institute of Animal Biochemistry and Genetics, Slovak Academy of Sciences, Bratislava, Slovakia

**Corresponding author**

Prof Dr Annemie Van der Linden

Address: Bio-Imaging Lab, UC 109
Universiteitsplein 1
2610 Wilrijk
Belgium

Telephone number: +32 3 265 27 75

Email address: annemie.vanderlinden@uantwerpen.be

**Summary of Declaration of Interests**

None

## Abstract

The first months of life are characterized by massive neuroplastic processes that parallel the acquisition of skills and abilities vital for proper functioning in later life. Likewise, juvenile songbirds learn the song sung by their tutor during the first months after hatching. To date, most studies targeting brain development in songbirds exclusively focus on the song control and auditory pathways. To gain a comprehensive insight into structural developmental plasticity of the entire zebra finch brain throughout the different subphases of song learning, we designed a longitudinal study in a group of male (16) and female (19) zebra finches. We collected T2-weighted 3-dimensional anatomical scans ~~(70 µm isotropic resolution)~~ at six developmental milestones throughout the process of song learning, i.e. 20, 30, 40, 65, 90 and 120 days post hatching (dph), and one additional time point well after song crystallization, i.e. 200 dph. We observed that the total brain volume initially increases, peaks around 30-40 dph and decreases towards the end of the study. Further, we performed brain-wide voxel-based volumetric analyses to create spatio-temporal maps indicating when specific brain areas increase or decrease in volume, relative to the subphases of song learning. These maps informed (1) that most areas implicated in song control change early, i.e. between 20 and 65 dph, and are embedded in large clusters that cover major subdivisions of the zebra finch brain, (2) that volume changes between consecutive subphases of vocal learning appear highly similar in males and females, and (3) that only more rostrally situated brain regions change in volume towards later ages. Lastly, besides detecting sex differences in local tissue volume that align with previous studies, we uncovered two additional brain loci that are larger in male compared to female zebra finches. These volume differences co-localize with areas related to the song control and auditory pathways and can therefore be associated to the behavioral difference as only male zebra finches sing. In sum, our data point to clear heterochronous patterns of brain development similar to brain development in mammalian species and this work can serve as a reference for future neurodevelopmental imaging studies in zebra finches.


## Graphical abstract (optional)

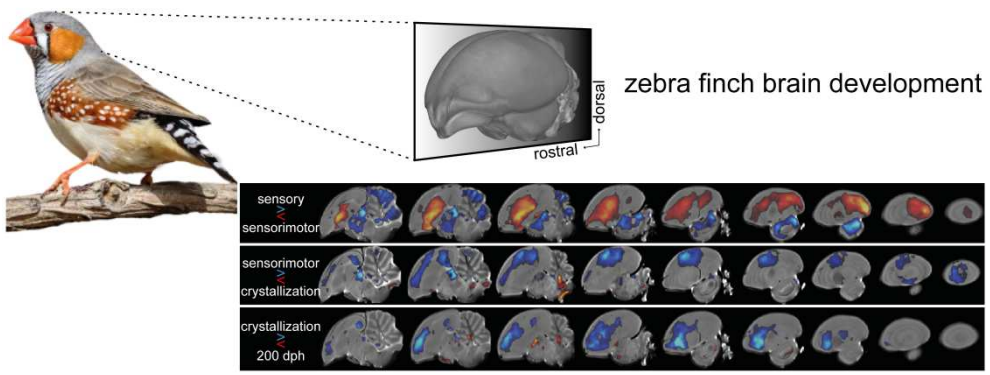

## Keywords

songbird – brain development – morphometry – zebra finch – MRI

## Abbreviations

| | |
|---|---|
| AFP | anterior forebrain pathway |
| CMP | caudal motor pathway |
| CM | caudal mesopallium |
| DLM | medial part of the dorsolateral nucleus of the anterior thalamus |
| dph | days post hatching |
| HVC | abbreviation used as a proper name (high vocal centre) |
| ICo | intercollicular nucleus |
| LMAN | lateral magnocellular nucleus of the anterior nidopallium |
| NIf | interfacial nucleus of the nidopallium |
| MLd | dorsal part of the lateral mesencephalic nucleus |
| RA | robust nucleus of the arcopallium |
| TeO | optic tectum |
| tOM | occipitomesencephalic tract |
| TSM | septomesencephalic tract |

# 1 Introduction

The first months of life are characterized by extensive neuroplastic processes that coincide with sensitive and critical periods of development during which skills and abilities necessary for proper functioning later in life are mastered (Knudsen 2004). A remarkable model in the study of developmental neuroplasticity related to complex skill acquisition can be found in songbirds. More specifically, juvenile zebra finches learn to produce the song sung by an adult conspecific during a well-defined developmental time window situated within the first 4 months of life (Immelmann 1969, Tchernichovski et al. 2001). This critical period for song learning consists of two partly overlapping subphases. First, during the sensory phase (appr. 25 to 50 days post hatching (dph)), juvenile birds memorize a specific song sung by an adult male (tutor). Next, during the sensorimotor phase (appr. 40 to 90 dph), the juveniles will 'trial-and-error' practice trying to match their own vocalizations to the previously memorized tutor song. Reaching the end of the sensorimotor phase, zebra finch song will 'crystallize' (appr. 90-120 dph) implying that their song will become 'fixed' and, in normal circumstances, will remain unchanged. Decades of research have highlighted numerous parallels in the genes, neural network architecture and behavioral process characterizing human speech and bird song learning, making songbirds –especially zebra finches– currently the most suitable animal model to study aspects of human speech acquisition in early life and speech motor control and maintenance in adulthood (Bolhuis et al. 2010, Brainard et al. 2013, Ziegler et al. 2017).

The songbird brain is structured fundamentally different compared to the mammalian brain (Nottebohm 1980, Reiner et al. 2004). Instead of a laminar structure, i.e. cortical layers, grey matter is organized into nuclei. Each nucleus connects to other nuclei via fiber tracts. This way extensive circuitries are formed, of which the auditory and song control system respectively underlie audition and song production. The song control system consists of two main pathways, i.e. the caudal motor (CMP) and anterior forebrain pathway (AFP), which are involved in distinct aspects of song performance. The CMP connects two cortex-like areas, i.e. HVC (abbreviation used as a proper name) and the robust nucleus of the arcopallium (RA), and mainly controls vocal motor production (Simpson et al. 1990, Wild 1997). The AFP forms an indirect connection between HVC and RA, similar to the cortico-basal ganglia-thalamo-cortical loop implicated in speech motor control in humans (Ziegler et al. 2017). More specifically, the ~~AFP sequentially connects HVC, Area X (shares structural and functional similarities with the mammalian basal ganglia (Reiner et al. 2004, Person et al. 2008)), the medial part of the dorsolateral nucleus of the anterior thalamus (DLM; thalamic region), the lateral magnocellular nucleus of the anterior nidopallium (LMAN; cortex-like region) and RA. The~~ AFP is involved in trial-and-error vocal exploration in ontogeny and song maintenance in adulthood (Brainard et al. 2000, Brainard 2004, Perkel 2004). Importantly, only male zebra finches produce songs and this behavioral difference is reflected in the neural substrate underlying song performance as Area X (component of the AFP), HVC and RA are larger in males compared to females (Nottebohm et al. 1976, Nixdorf-Bergweiler 1996, MacDougall-Shackleton et al. 1999).

To date, most insights into the structural architecture of the zebra finch brain have mainly been obtained using invasive methods such as histology. These methods are extremely sensitive and specific, however, they strongly interfere with obtaining repeated-measures over extended time frames (i.e. weeks or months) in the same subject and often limit the area of investigation to *a priori* defined regions-of-interest (ROIs). As a result, most research is exclusively focused on the traditionally studied song control and auditory system, leaving the rest of the brain underexplored. In humans and rodents, MRI emerged as a prominent tool to quantify adaptations to brain structure that arise over development, e.g. (Lebel et al. , Giedd et al. 1999, Gogtay et al. 2004, Calabrese et al. 2013, Calabrese et al. 2013, Mengler et al. 2014, Raznahan et al. 2014, Hammelrath et al. 2016). Indeed, automated volumetric analyses or assessments of cortical thickness have led to the establishment of regionally-specific developmental trajectories in several species (Gogtay et al. 2004, Dubois et al. 2014). Such stereotyped patterns of brain maturation yield important functional implications reminiscent of critical and sensitive periods as cognitive milestones are reached in parallel with structural neuroplastic events (Knudsen 2004).

Inspired by these imaging studies, we set out to explore the timing and spatial extent of volume changes affecting the zebra finch brain at different stages along the process of vocal learning. To this end, we obtained T2-weighted 3-dimensional (3D) anatomical scans at seven time points coinciding with developmental milestones relative to the critical period of vocal learning, i.e. during the sensory (20 and 30 dph), sensorimotor (40 and 65 dph) and crystallization phase (90 and 120), and past the critical period for vocal learning (200 dph), in 16 male and 19 female zebra finches. The T2-weighted 3D anatomical scans were processed for voxel-based volumetric analyses, termed deformation-based morphometry (DBM) (Ashburner et al. 2012, Ashburner et al. 2015). Exploiting the advantages of *in vivo* MRI, we performed brain-wide voxel-wise statistical analyses to quantitatively explore gross anatomical differences in size that arise between both sexes, which by comparison to established findings in songbird literature served to validate the processing pipeline, or as a consequence of age. As such, this study is the first to target the structural development of the zebra finch brain *in vivo*.

# 2 Material and Methods

## 2.1 Animals and Ethical statement

Male (n = 16) and female (n = 19) zebra finches (*Taeniopyiga guttata*) were bred in the local animal facility. Only birds with a grey phenotype were included in this study, as white plumage morphs have been shown to display functional alterations in the visual system (Bredenkotter et al. 1996). The birds were housed in individual cages together with an adult male, an adult female and one or two other juvenile birds. The ambient room temperature and humidity were controlled, the light-dark cycle was kept constant at 12h-12h, and food and water was available *ad libitum* at all times. In addition, from the initiation of the breeding program until the juvenile birds reached the age of 30 days post hatching (dph), egg food was provided as well. The Committee on Animal Care and Use at the University of Antwerp (Belgium) approved all experimental procedures (permit number 2012-43 and 2016-05) and all efforts were made to minimize animal suffering.

## 2.2 MRI data acquisition

We acquired 3-dimensional Rapid Acquisition with Relaxation Enhancement (3D RARE) in male and female zebra finches at 20, 30, 40, 65, 90, 120 and 200 dph. We strived for maximal accuracy of the age of acquisition (relative errors of age at acquisition are: 1.39% at 20, 0.73% at 30, 1.15% at 40; 0.97% at 65, 0.84% at 90, 0.78% at 120, and 0.61% at 200 dph). All MRI data were acquired on 7 T horizontal MR system (PharmaScan, 70/16 US, Bruker BioSpin GmbH, Germany) combined with a quadrature transmit volume coil, linear array receive coil designed for mice, and a gradient insert (maximal strength: 400 mT/m; Bruker BioSpin, Germany). In brief, first, the zebra finches were

anesthetized with isoflurane (IsoFlo®, Abbott, Illinois, USA; induction: 2.0-2.5%; maintenance: 1.4-1.6%). After collecting $T_2$-weighted Turbo RARE pilot scans to enable uniform slice positioning across imaging sessions, a $T_2$-weigthed 3D RARE dataset was obtained with the following settings: TE 11 ms ($TE_{eff}$ 55 ms), TR 2500 ms, RARE factor 8, FOV (18x16x10) $mm^3$, acquisition matrix (256x92x64) zero-filled to (256x228x142) for reconstruction yielding an isotropic voxel dimension (0.07 mm)$^3$~~, spatial resolution (0.07x0.17x0.16) $mm^3$ zero-filled to (0.07x0.07x0.07) $mm^3$~~, scan duration 29 min. The FOV of the 3D RARE scan captured the entire zebra finch brain.

Throughout the entire imaging procedure, the birds' physiological condition was monitored closely by means of a pressure sensitive pad placed under the chest of the bird to detect the breathing rate, and a cloacal thermistor probe connected to a warm air feedback system to maintain the birds' body temperature within narrow physiological ranges (40.0 ± 0.2) °C (MR-compatible Small Animal Monitoring and Gating system, SA Instruments, Inc). All animals recovered uneventfully within a few minutes after discontinuation of the anesthesia.

### 2.3 MRI data processing

The 3D RARE datasets were pre-processed to enable voxel-wise statistical testing to highlight brain areas that display a difference in relative volume between both sexes or over consecutive developmental stages. Voxel-wise detection of local volume differences between groups or over time relies on image registration which refers to the spatial transformations that define how one image should be spatially changed to overlap with another image. Several spatial registration methods are available (Klein et al. 2009), however, in case of a longitudinal study design with repeated measures a different registration strategy should be adopted to avoid processing-induced registration biases (Reuter et al. 2012). We have employed a similar two-step procedure including first a within-subject spatial registration to map age-related changes in local tissue volume (Ashburner et al. 2012), and second a between-subject registration to account for local volume differences existing between different subjects (Ashburner 2007). Figure 1 presents an overview of the different processing steps, which were performed in the following software packages: SPM12 (Statistical Parametric Mapping, r 6225, Wellcome Trust Centre for Neuroimaging, London, UK, http://www.fil.ion.ucl.ac.uk/spm/) supplemented with the DARTEL toolbox (Ashburner 2007), Amira (v5.4.0, FEI; https://www.fei.com/software/amira-3d-for-life-sciences/), ANTs (Advanced Normalization tools; (Avants et al. 2011); http://stnava.github.io/ANTs/) and FSL (FMRIB Software Library; (Jenkinson et al. 2012); https://fsl.fmrib.ox.ac.uk/fsl/fslwiki/FSL).

### 2.3.1 Deformation-based morphometry

First, the individual 3D RARE scans were masked (Amira v5.4.0) so that the resulting images only contained the brain. This manual brain extraction was performed blind to sex and appeared necessary as for the youngest ages (20-40 dph), the spatial registration procedures failed to correctly distinguish between the rostral parts of the brain, meninges and skull. This resulted in suboptimal subsequent image registration near the most rostral part of the telencephalon. Secondly, one average 'within-subject' 3D dataset (midpoint average) was created for each animal based on the seven individual, masked 3D RARE scans acquired at the different ages using the serial longitudinal registration (SLR) tool of SPM12 (Ashburner et al. 2012). Supplementary Information SI-2 describes the registration accuracy of this procedure. Besides the midpoint average, the SLR generated jacobian determinant (j) maps, divergence of velocity (dv) maps and deformation fields. Next, the midpoint averages of all animals were inputted in the 'buildtemplateparallel' function of the Advanced Normalization Tools (ANTs; (Avants et al. 2008, Avants et al. 2011)). The resulting 'between-subject' population-based 3D was used by the FMRIB Automated Segmentation Tool (FAST; (Zhang et al. 2001)) embedded in FSL, to extract tissue probability maps reflecting mainly grey matter ($c_1$), white matter ($c_2$) and cerebrospinal fluid ($c_3$), using the default settings for $T_2$-weighted datasets (an example of the resulting segments can be found in Figure 3). The three tissue class probability maps created in FAST were used for segmenting the individual midpoint averages using the default settings of the (old)segment batch in SPM12. Then, the within-subject 3D segments were inputted in DARTEL to create a segment-based population-based template (Ashburner 2007, Ashburner et al. 2009). Important to note is that in future studies, several image processing steps presented here can be omitted. Since no tissue segments of the zebra finch brain were available, we chose to create tissue segments based on one single dataset using FAST and further refine the tissue segments estimated in FAST by creating a population-based tissue segment template in Dartel. We can make the population-based tissue segment template generated in Dartel available upon request. As a result, future studies will be able to directly segment the midpoint averages and proceed to Dartel without having to create a population-based template in ANTs, or tissue segments in FAST.

Next, the ANTs-based $T_2$-weighted template (only the T2-weighted dataset and not the derived tissue segments) was warped via the 'DARTEL: existing template' batch to spatially match with the segment template. The resulting DARTEL-ANTs population-based template was used as anatomical reference space for all voxel-based statistical analyses (and is from here onwards termed 'population-based template'). The flow fields produced by DARTEL encode the spatial transformation parameters to warp the midpoint average to the reference space and were applied to the jacobian determinant maps (with modulation) and divergence of velocity (without

modulation) that were previously produced during the SLR step. Applying the spatial transformations encoded in the flow fields "with modulation" refers to a voxel-by-voxel rescaling (multiplication) of the jacobian determinant or divergence of velocity maps with the jacobian determinant of the deformation. As a result, the modulation step serves to preserve relative volume differences existing between different subjects. Warping the jacobian determinant maps outputted by the SLR with modulation enables to test for between- and within-subject volume differences. We chose to warp the divergence of velocity maps without modulation as they were only used to highlight which brain areas drive the age-dependent (within-subject) increase and decrease in whole brain volume (SI-1).

Lastly, the warped modulated jacobian determinant maps were smoothed ~~in plane~~ using a Gaussian kernel with FWHM (0.14x0.14x0.14) $mm^2$.

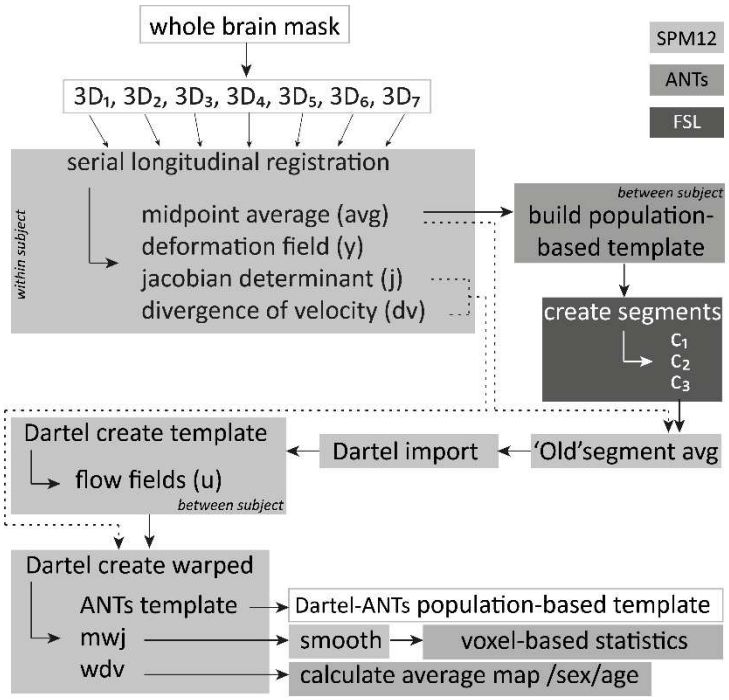


**Figure 1: Schematic overview of the processing pipeline of the 3D RARE (top) data.** A detailed description can be found in the text.

### 2.3.2 Volumetry of brain compartments

Whole brain volume was estimated by performing a back-transform of the mask delineated on the population-based template. The segment volume was obtained by projecting the tissue segments estimated on the midpoint averages to the native space. Each back-transformation was performed in one step (one interpolation), either by applying the inverse of the deformation fields estimated by the SLR (segments) or by combining the flow fields and deformation fields estimated by resp. Dartel and the SLR (composition; whole brain mask). The volumes of the back-transformed masks were

extracted via the 'get_totals' function in SPM12 (whole brain and segments) or using Matlab (version R2016b; MathWorks, Natwick, MA, USA).

### 2.4 Statistical analyses

Visual inspection of the raw data informed that two of the four animals displayed excessively large ventricles at the 20 dph time points and appeared normal thereafter. The other two animals showed an abnormal cerebellar folding pattern. These brain abnormalities would result in suboptimal image registration and, therefore, these four animals were excluded for voxel-based analyses, leaving 15 males and 16 females for DBM.

#### 2.4.1 Voxel-based analysis

***Interactions and main effects***

All voxel-wise statistical tests were executed in SPM12. Firstly, repeated-measures ANOVA's were performed on the smoothed, modulated jacobian determinant maps, including 'subject' as random factor, and 'sex' and 'age' as fixed factors and a covariate describing the whole brain volume. This design allowed for testing within-subject effects including interactions (age*sex) and main effects (age). Secondly, 2-sample T-tests were performed on the smoothed modulated jacobian determinant ~~parameter~~ maps ~~pooled from 120 and~~ obtained at 200 dph to explore sex differences that only arise towards adulthood –after the critical period for vocal learning has closed– and therefore might be missed by the interaction.

To further clarify when in time most extensive neuroplastic changes occur, hypothesis-driven F-tests comparing consecutive time points or successive subphases of vocal learning were executed. ~~Unless explicitly stated,~~ Only clusters that survived a family-wise error (FWE) correction thresholded at $p_{FWE}<0.05$ combined with a minimal cluster size ($k_E$) of at least 20 voxels were considered significant for the repeated-measures ANOVA. The 2-sample T-test of data obtained at 200 dph was assessed at $p_{uncorrected}<0.001$ and $k_E \geq 20$voxels. All statistical maps are displayed overlaid onto the population-based template. Figure ISI-2 provides an overview of the anatomical structures detectable on sagittal and horizontal slices of the population-based template.

***Post hoc testing of clusters detected by voxel-based analyses***

Clusters detected by the voxel-based analysis that displayed a significant interaction between age*sex, changes over time or between both sexes were converted to ROIs ('cluster-based ROIs') of which the mean modulated jacobian determinant, or (relative) volume (via backprojection to native space) were extracted for *post hoc* statistical testing in JMP® software (Version 13, SAS Institute Inc., Cary, NC, 1989-2007). First, a linear mixed model (restricted maximum likelihood) was selected to

confirm the presence of an interaction or main effect ('subject': random variable, 'age' and 'sex': fixed variables; total brain volume was not added as a covariate in the model). Significance was assessed using an F-test with Kenward-Roger approximation. Next, *post hoc* tests using Tukey's HSD (Honest Significant Difference) were used to situate which time points differed significantly.

# 3 Results

~~We strived for maximal accuracy of the age of acquisition (relative errors of age at acquisition are: 1.39% at 20, 0.73% at 30, 1.15% at 40; 0.97% at 65, 0.84% at 90, 0.78% at 120, and 0.61% at 200 dph).~~

## 3.1 Sex differences in local tissue volume

The results of the statistical tests exploring sex differences in local volume are summarized in Table 1 and Figure 2. The voxel-wise repeated-measures ANOVA of the smoothed, modulated jacobian determinant maps identified an interaction between age and sex at several clusters in various locations in the brain. The most significant cluster was localized near the occipitomesencephalic tract (tOM) at the level of the thalamus (Figure 2-A) and more ventrally near the intercollicular nucleus (ICo; Figure 2-C). At an exploratory statistical threshold ($p_{uncorrected}$<0.001; $k_E$≥100 voxels), the latter cluster extends towards the di- and mesencephalon (specifically to ICo) and more caudally towards the cerebellum. When exploring the spatial extent of the cluster even more *liberally* ($p_{uncorrected}$<0.01; $k_E$≥100 voxels), the ventral tOM cluster connects to the cluster covering the tOM near the thalamus (data not shown). Furthermore, three song control nuclei i.e. area X of the left hemisphere (Figure 2-B), HVC (Figure 2-D), and RA of the right hemisphere (Figure 2-E) were found to display a sex-dependent volumetric trajectory over time as well. No clusters could be observed co-localized with the left RA, left HVC and right Area X, when testing for an interaction between age and sex.

The 2-sample T-test including datasets obtained ~~at 120 and~~ 200 dph uncovered overall similar clusters, but additionally identified a significant volume difference near the ventral portion of Field L potentially co-localizing with the interfacial nucleus of the nidopallium (NIf, Figure 2-F). ~~At a lower statistical threshold, i.e. $p_{uncorrected}$<0.001 $k_E$≥20 voxels, bilateral clusters covering major parts of the arcopallium (including RA), HVC and LMAN were uncovered (data not shown).~~ No suprathreshold clusters were found presenting a higher volume in females compared to males at ~~120 and~~ 200 dph.

**TABLE 1: Clusters displaying an interaction or a sex difference in local tissue volume.**

| Statistical test | Cluster-based ROI | | Cluster level | | Peak level | |
|---|---|---|---|---|---|---|
| | | | $p_{FWE}$ | $k_E$ | $p_{FWE}$ | *F* or *T* |
| Interaction age*sex | tOM near thalamus | Left | <0.001 | 183 | <0.001 | 17.22 |
| | | Right | <0.001 | 79 | <0.001 | 13.09 |
| | HVC | Left | . | . | . | . |
| | | right | <0.001 | 109 | <0.001 | 12.00 |
| | tOM near ICo | Left | <0.001 | 220 | <0.001 | 10.63 |
| | | Right | <0.001 | 212 | <0.001 | 11.66 |
| | Area X | Left | <0.001 | 396 | 0.001 | 9.69 |
| | | Right | . | . | . | . |
| | RA | Left | . | . | . | . |
| | | Right | 0.002 | 43 | 0.003 | 9.15 |
| M > F (~~120 &~~ 200 dph) | Ventral part of Field L | Left | ~~0.004~~ . | ~~32~~ . | ~~0.001~~ . | ~~6.78~~ 4.61 |
| | | Right | ~~0.001~~ . | ~~61~~ . | ~~0.001~~ . | ~~6.64~~ 4.71 |

'Interaction age*sex' was performed in a flexible factorial design and serves to unveil brain regions that display a sex-dependent trajectory, while the 'M>F (~~120 &~~ 200 dp~~j~~h)' is extracted from a 2-sample T test including datasets obtained at ~~120 and~~ 200 dph and informs on areas that display volume differences between both sexes. The 'Cluster level' and 'Peak level' columns refer to respectively the *p*-value (after 'Family Wise Error' correction for multiple comparisons) of the clusters and cluster extent ($k_E$), and *p*- and *F*-values of the peak voxel of the clusters provided by SPM. Since the statistical parametric maps of the two-sample T test were assessed without FWE correction, no cluster-level statistics or peak $p_{FWE}$ are reported. The '.' indicates that no cluster or no significant differences could be observed in this region at $p_{FWE}$<0.05 $k_E$≥20 voxels. Abbreviations: tOM: occipitomesencephalic tract; RA: robust nucleus of the arcopallium; HVC: abbreviation used as proper name.

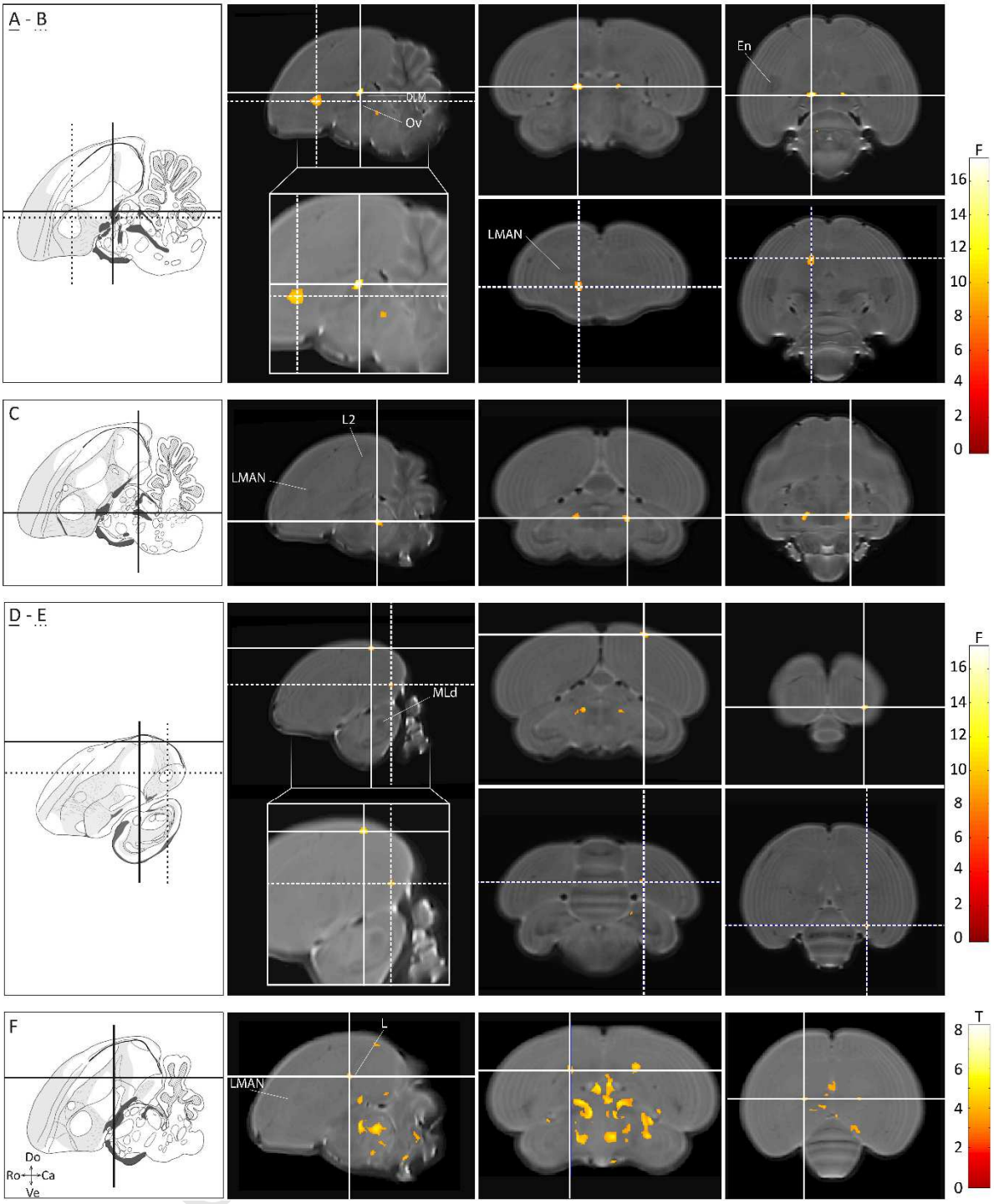


**Figure 2: Sex differences in local tissue volume.** Statistical Parametric Maps illustrating the spatial extent of the clusters observed by the interaction between age*sex (panel A-E) or a main effect of sex (panel F). The crosshairs converge on (**A**) tOM near the thalamus, (**B**) left Area X, (**C**) tOM near ICo, (**D**) right HVC, (**E**) right RA, and (**F**) the ventral portion of Field L potentially co-localized with NIf. The results of panel A-E are displayed $p_{FWE}$<0.05 $k_E$≥20 voxels and of panel F $p_{uncorrected}$<0.001 $k_E$≥20 voxels, overlaid on the population-based template, and color-coded according to the scales on the right (F or T-values). The atlas drawings on the left –obtained from the zebra finch histological atlas browser (Oregon Health & Science University, Portland, OR 97239; http://www.zebrafinchatlas.org (Karten et al. 2013)– were taken at approximately the same lateral position as the sagittal MR image immediately adjacent to it. Abbreviations: Do: dorsal; Ve: ventral; Ro: rostral; Ca: caudal.

The clusters that displayed an interaction and/or an overall sex difference in the voxel-wise analysis were converted to ROIs, of which the average modulated jacobian determinant value was extracted and subjected to *post hoc* statistical testing (Tukey's HSD) to situate when in time the actual difference establishes. For all ROIs, except for the cluster co-localized with the ventral portion of Field L possibly including NIf, the significant interaction between age and sex was confirmed by a linear mixed model (HVC right: $p$=0.0020 $F_{(6,186.0)}$=3.6358; RA right: $p$=0.0005 $F_{(6,186.0)}$=4.2766; Area X left $p$=0.0003 $F_{(6,186.0)}$=4.4707; part of the tOM near the thalamus left $p$<0.0001 $F_{(6,186.0)}$=18.1338; part of the tOM near the thalamus right $p$<0.0001 $F_{(6,186.0)}$=9.6597; ventral part of the tOM cluster left $p$<0.0001 $F_{(6,186.0)}$=14.4741; ventral part of the tOM cluster right $p$<0.0001 $F_{(6,186.0)}$=14.6646; ventral portion of Field L or Nif right: $p$=0.1202 $F_{(6,186.0)}$=1.7125; left: $p$=0.7961 $F_{(6,186.0)}$=0.7961). Importantly however, the clusters near the ventral portion of Field L displayed a clear sex difference in volume (main effect of sex: right: $p$=0.0119 $F_{(1,31.0)}$=7.1427; left: $p$=0.0182 $F_{(1,31.0)}$=6.2189). Figure ISI-1 provides details on nature of the interaction between age and sex, or main effect of sex extracted from the cluster-based ROIs.

[Insert inline supplementary figure 'Figure ISI-1' here]

### 3.2 Brain-wide volume changes

The previous analyses clearly show that several anatomical areas related to the auditory and song control system display structural sex differences. Consequently, testing for structural changes over the different ages was performed for each sex separately.

#### 3.2.1 Segmenting modular instead of laminar brains

Even though the bird brain differs fundamentally from the mammalian brain, the FAST tool of FSL ~~managed to~~ discriminated three different tissue classes on the population-based template built in ANTs, i.e. $c_1$ containing mostly grey matter areas, $c_2$ including the majority of white matter structures and $c_3$ encompassing mostly CSF. Figure 3 illustrates the resulting tissue probability maps.

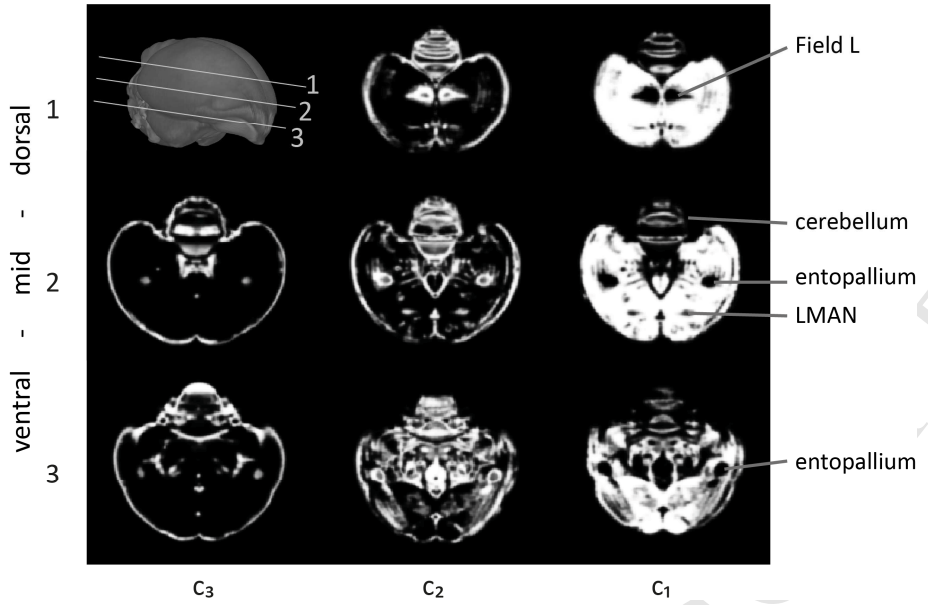


**Figure 3: Overview of the tissue segments.** The top left corner presents a 3D-rendered view of the population-based template that indicates the location at which the three different horizontal slices were obtained (1, 2 and 3 or dorsal, mid and ventral).

### 3.2.2 Volumes of brain compartments

The total brain volume and volume of the tissue compartments were determined by back-projecting the 'whole brain mask' from the template and the segments made on the average 3D produced during the SLR step to the individual datasets in native space and extracting the volumes of the back-projected masks using the 'get_totals' function of SPM. Next, the relative segment volumes were calculated (((absolute segment volume)/(sum of the segments of the corresponding time point))*100). The linear mixed model identified an interaction between age*sex for the whole brain volume ($F_{(6,186.0)}$= 5.6735; $p$<0.0001), but not for relative $c_1$, $c_2$, and $c_3$ volumes ($F_{(6,186.0)}$= 0.5597; $p$=0.7620; $F_{(6,186.0)}$= 0.8598; $p$=0.5265; $F_{(6,186.0)}$= 1.589; $p$=0.1589 respectively). The three segments did show a significant main effect of time ($c_1$: $F_{(6,192.0)}$= 119.5394 $p$<0.0001; $c_2$: $F_{(1,192.0)}$= 139.0462 $p$<0.0001; $c_3$: $F_{(6,192.0)}$= 67.7312 p<0.0001), and a weak main effect of sex was observed for $c_2$ and $c_3$ ($c_1$: $F_{(1,31.0)}$= 0.0238 $p$=0.8785; $c_2$: $F_{(1,31.0)}$= 4.3850 $p$=0.0445 M>F; $c_3$: $F_{(1,31.0)}$= 4.5859 $p$=0.0402 M<F). The results of the *post hoc* tests (Tukey HSD) are summarized in Figure 4.

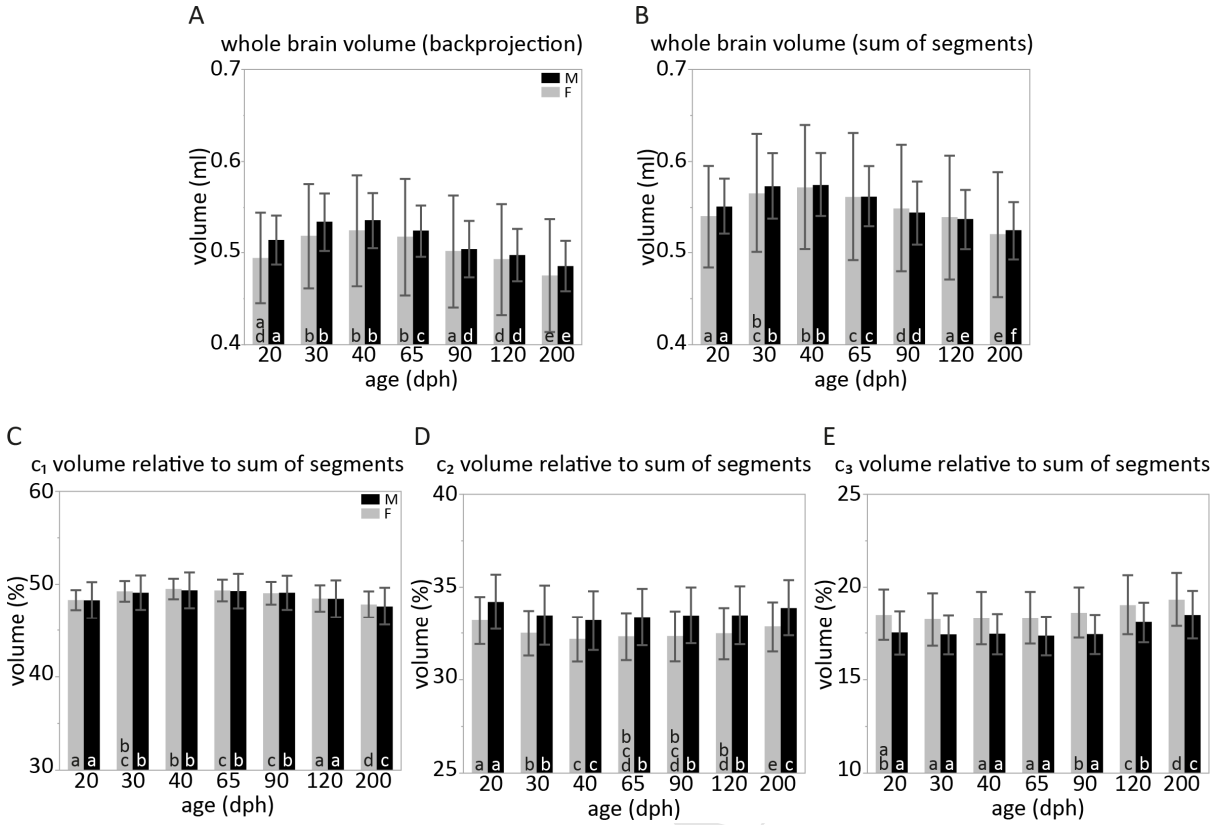


296

297 **FIGURE 4: Whole brain and tissue compartment volume in function of age.** The bar graphs illustrate the volume of the
298 entire brain (A-B) and the volumes of the different segments, i.e. $c_1$ (C), $c_2$ (D) and $c_3$ (E), for male (black) and female (grey)
299 zebra finches, in function of age. The bars indicate the mean ± standard deviation. The black or white letters at the base of
300 each bar refer to the results of the post hoc test (Tukey HSD) to inform when in time volume changes occur, for males or
301 females respectively. If two time points share the same letter, then the volumes do not differ between both ages. For
302 example, a bar containing 'a' is not significantly different from any other bar that contains 'a' or a combination of letters
303 that includes 'a', but is statistically different from all bars that do not contain 'a' (e.g. 'bc'). In female birds, whole brain
304 volume at 20 dph (a,d) differs significantly from whole brain volume at 30 (b), 40 (b), 65 (b) and 200 (e) dph, but not from
305 90 (a) and 120 (d) dph. Abbreviations: dph: days post hatching.

306 To obtain spatial information which brain areas primarily drive the initial increase and later decrease
307 in total brain volume, we calculated for each time-point and sex separately an average divergence of
308 velocity (dv) map. The results are presented in the Supplementary Information (Figure SI-1).
309 Furthermore, Supplementary Information Figure SI-2 provides an overview of age- and sex-specific
310 population-based templates to illustrate the overall shape and volume of the brain relative to the
311 other ages and sex.

312 **3.3 Brain-wide voxel-wise statistical analyses to explore localized volume changes over time**

313 We performed a voxel-wise repeated-measures ANOVA (random effect for 'subject', fixed effects for
314 'age' and 'sex'; covariate for whole brain volume) on the jacobian determinant maps. The main
315 effect of age informs that almost the entire brain displays relative volume changes from 20 to 200

dph (Figure 5). This concurs with the whole brain volume estimates (Figure 4) that present an initial increase and later decrease. Figure ISI-2 facilitates the identification of anatomical areas or brain subdivision of the brain slices included in Figure 5-6.

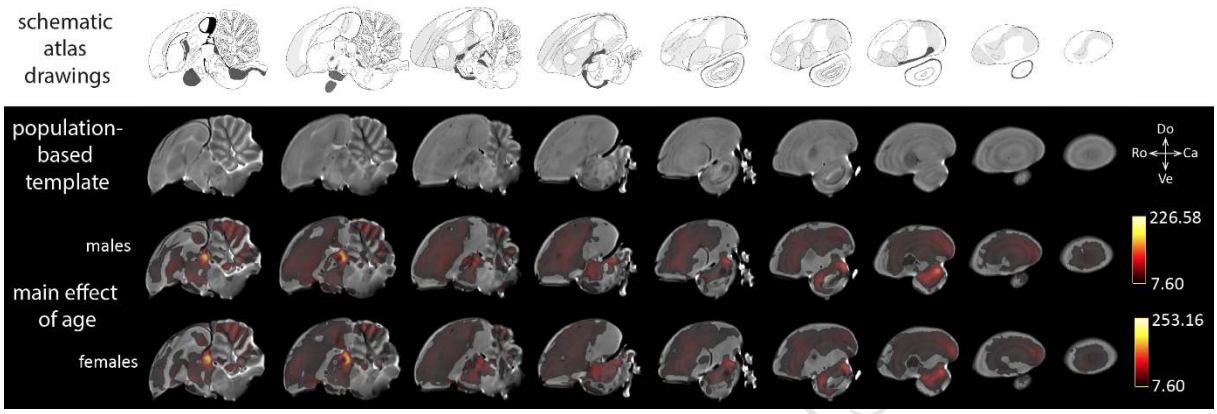


**FIGURE 5: Brain-wide changes in local volume during the first 200 days of post-hatch life.** The spatial extent of the clusters covers similar areas in the male and female zebra finch brain. The SPMs are displayed according to $F>7.60$ which corresponds to $p_{FWE}<0.05$ (color-code on the right of each set of sagittal images), and overlaid on the population-based template. The atlas drawings on top–obtained from the zebra finch histological atlas browser (Oregon Health & Science University, Portland, OR 97239; http://www.zebrafinchatlas.org (Karten et al. 2013)– were taken at approximately the same lateral position as the sagittal MR image immediately below. Figure ISI-2 present anatomical labels on the slices underlying the statistical maps. Abbreviations: Do: dorsal; Ve: ventral; Ro: rostral; Ca: caudal.

Next, hypothesis-driven *post hoc* tests comparing the different sub-phases of vocal learning (Figure 6) indicated that when contrasting the sensory (20-30 dph) and the sensorimotor (40-65 dph) phase, several areas of the telencephalon, thalamic structures and the optical lobes (optic tectum (TeO); anatomical overview in Figure ISI-2) display significant volume changes, both in males and females. The cluster in the telencephalon increases in volume towards the sensorimotor phase and covers major parts of the striatum containing Area X, LMAN, and extends dorso-caudally and laterally towards areas in the nido- and mesopallium. Interestingly, the clusters covering the thalamus and the mesencephalon (optic lobes) and cerebellum appear to decrease in volume from the sensory to the sensorimotor phase. When comparing the sensorimotor (40-65 dph) and crystallization phases (90-120 dph), again the thalamus (volume decrease) but also the lateral cerebellar nuclei (volume increase) and several clusters near the frontal parts of the telencephalon (i.e. apical and densocellular hyperpallium; volume decrease) including areas of the lateral, medial and caudal mesopallium (volume decrease) caudally demarcated by Field L could be observed. Furthermore, comparing the crystallization phase (90-120 dph) to the last time point (200 dph) informs that still several frontal parts of the telencephalon decrease in volume over time. However, as opposed to the previous comparison, the clusters appear to be focused in more ventral parts of the nido- and

mesopallium lateral and frontal to the striatum extending to the ventral parts of the caudal mesopallium. Interestingly, LMAN is clearly excluded from this cluster. Furthermore, except for a cluster that covers the nidopallium and potentially includes the rostral portion of Field L2, no song control and/or auditory areas were found to display a change in relative volume, which clearly contrasts earlier comparisons. In addition, also more anatomically discrete clusters covering the posterior commissure, a ventro-rostral extension of the tOM and the septomesencephalic tract (TSM) could be observed. All of which are characterized by a larger volume at 200 dph compared to 90 and 120 dph. Overall, the statistical maps of male and female birds showed similar effects over time when comparing the subphases of vocal learning (Figure 6).

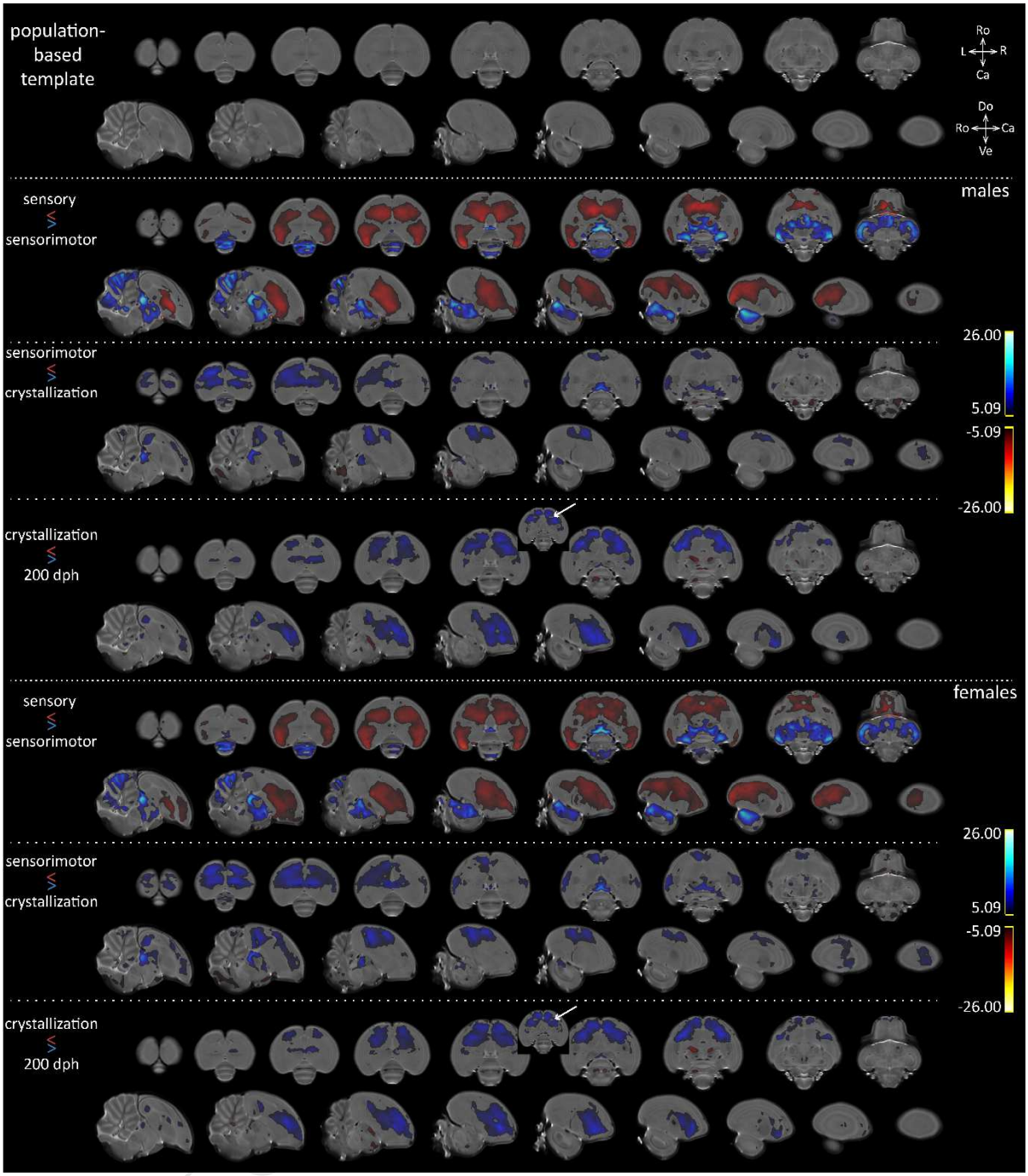


**Figure 6: Relative volume differences between consecutive subphases of vocal learning in male and female zebra finches.** The statistical maps highlight voxels where the modulated jacobian determinants are larger (blue: volume decrease from first to later phase) or smaller (red; expansion from first to later phase) at the sensory phase compared to the sensorimotor phase, sensorimotor compared to the crystallization phase, or around crystallization compared to 200 dph. The sensory phase includes data obtained at 20-30 dph, the sensorimotor phase 40-65 dph, and the crystallization phase 90-120 dph. The statistical maps are color-coded according to the scale on the right (T-values; T=5.09 corresponds to $p_{FWE}$<0.05, no cluster extent threshold). Figure ISI-2 present anatomical labels on the slices underlying the statistical maps. The white arrow in the horizontal slices points to LMAN. ~~The atlas drawings on top obtained from the zebra finch histological atlas browser (Oregon Health & Science University, Portland, OR 97239; http://www.zebrafinchatlas.org~~

(Karten et al. 2013) - were taken at approximately the same lateral position as the sagittal MR image immediately below.

Abbreviations: dph: days post hatching; Do: dorsal; Ve: ventral; Ro: rostral; Ca: caudal.

# 4 Discussion

The present study aimed at composing a brain-wide comprehensive overview of the timing and spatial extent of alterations in tissue volume along the first 200 days of post-hatch life in male and female zebra finches. Earlier studies have mainly used histological and/or genetic methods in cross-sectional study designs and exclusively focused on the song control and auditory pathways. Our work complements and extends these earlier reports by describing the first longitudinal *in vivo* MRI study in juvenile zebra finches. This experimental strategy enabled us to create a brain-wide spatiotemporal map displaying when particular areas expand or contract (Figure 6), reminiscent of waves of brain maturation reflected in changes in cortical thickness in mammals e.g. (Gogtay et al. 2004, Calabrese et al. 2013, Hammelrath et al. 2016). Further, brain-wide voxel-wise data analyses have revealed two additional previously unidentified sex differences in brain structure, both of which are part of the auditory and song control pathways.

## 4.1 *In vivo* detection of sex differences in local volume: validation of the protocol

Only male zebra finches sing. This behavioral contrast is mirrored in the neural substrate underlying singing behavior as many brain areas directly in control of singing, i.e. HVC, RA and Area X, are larger in males compared to females (Nottebohm et al. 1976). Most sex differences observed in this study (Figure 2) relate to areas in control of or tracts connecting different nuclei involved in song behavior and corroborate with zebra finch literature (MacDougall-Shackleton et al. 1999). More specifically, we observe clear sex differences in local volume near HVC, Area X (left), RA (right), at two levels of the tOM (near the thalamus and near the ICo) and the ventral portion of Field L co-localizing with the NIf (Figure 2). Sex-dependent volume differences in HVC, RA and Area X are very well known (Nottebohm et al. 1976) and previous studies have shown that sex differences in the volume of these areas should be fully established by 60 dph (Nixdorf-Bergweiler 1996).

To our knowledge, the sex-dependent volume difference near the ventral part of Field L, co-localizing with the NIf, is a novel finding. Besides the reciprocal connection with the Avalanche nucleus (Akutagawa et al. 2010), the NIf is the main auditory afferent of HVC, an important 'relay' center of the song control system (Coleman et al. 2007). Furthermore, the NIf exhibits both auditory and vocal-motor activity (Lewandowski et al. 2011) and drives sleep-related replay of premotor activity in HVC (Hahnloser et al. 2007). Lesion and inactivation studies provide evidence of the active involvement of NIf in sensorimotor learning and song production (Naie et al. 2011, Roberts et al. 2012). In contrast, adult song production appears less impacted in case of bilateral lesioning of NIf

(Cardin et al. 2005). Based on these and other findings (reviewed by (Lewandowski et al. 2013)), we propose that our finding (volume of NIf M>F) adds to the generally accepted sex differences in volume described for areas pertaining to the song control system (Nottebohm et al. 1976).

### 4.2 Brain volume resembles an inverted U-shape

Both in males and females, whole brain volume increases between 20 and 30 dph, remained constant between 30 and 40 dph and progressively decreased from 40 dph towards the end of the study. This finding corroborates with and extends previous estimations of increasing telencephalon size between 12 and 53 dph in male and female zebra finches (Bottjer et al. 1997). The temporal pattern, i.e. initial increase and later decrease, greatly resembles the inverted U-shaped trajectory described in humans where total brain volume initially increases, peaks in adolescence and gradually declines towards adulthood, e.g. (Giedd et al. 1999, Gogtay et al. 2004, Lenroot et al. 2007, Group. 2012), for review (Giedd et al. 2014, Mills et al. 2014, Morita et al. 2016). In contrast, other small animal species displayed distinctly shaped brain volume trajectories e.g. mice (Zhang et al. 2005, Chuang et al. 2011, Hammelrath et al. 2016), rats (Calabrese et al. 2013, Calabrese et al. 2013, Mengler et al. 2014), and cats (Rathjen et al. 2003). Important to note is the age-range included in the study, as a potential volume decline might only affect older ages.

### 4.3 Regionally-specific developmental trajectories

Automated volumetric analyses or assessments of cortical thickness in function of age have led to the establishment of regionally-specific developmental trajectories in several species, e.g. (Gogtay et al. 2004). These stereotyped patterns of brain maturation yield important functional implications reminiscent of critical and sensitive periods as cognitive milestones are reached in parallel with structural neuroplastic events (Knudsen 2004). We employed a similar research strategy and created SPMs highlighting brain areas that display a volume change when comparing consecutive subphases of vocal learning (Figure 6). Effects of time were assessed in male and female finches separately, but resulted in highly similar overall maturational patterns. Males and females display early widespread changes covering the entire telencephalon and later neuroplastic alterations mainly affecting more rostral parts of the nido- and mesopallium.

#### 4.3.1 Sensory vs sensorimotor

When contrasting the sensory and sensorimotor sub-phases, we observe a volume increase in parts of the striatum, meso- and nidopallium, and a volume decrease in the optic lobes, parts of the cerebellum and thalamic zone (Figure 6; Figure ISI-2 presents an overview of the songbird brain anatomy). More specifically, the optic tectum and the dorsal part of the lateral mesencephalic nucleus (MLd) located in the optic lobes decrease in volume between 20 and 30 dph (data not

shown). The TeO receives direct input from both eyes, connects to various sensory and sensorimotor areas throughout the bird brain, and appears therefore closely implicated in the processing of visual information (Bischof et al. 1990). MLd is the songbird analogue of the mammalian inferior colliculus and the amphibian torus semicircularis, is an important 'early' auditory relay center as several parallel auditory brainstem pathways converge in this nucleus (Wild 1995), and it receives descending input from the $HVC_{shelf}$ and $RA_{cup}$ regions (Wild et al. 1993). The latter pathway might serve to convey song-related feedback to the MLd. MLd is tonopically organized, displays selectivity for particular spectro-temporal features (Woolley et al. 2005), with great sensitivity to temporal patterns characteristic to bird songs (Woolley et al. 2006) and expresses the IEG 'zenk' following passive song playback (Mello et al. 1998). The relative volume change in MLd occurs at the earliest stages of vocal learning when juvenile birds memorize the tutor song. Furthermore, the HVC-RA connection exhibits marked changes in both sexes taking place between 20 and 30 dph (Konishi et al. 1985, Holloway et al. 2001), which potentially –via shelf and cup pathways– may affect the structure of MLd.

The volume increase that includes the striatum and the medial meso-and lateral nidopallium envelops Area X and LMAN (less so in female birds), two important components of the song control system. Despite the clear sex difference in volume of Area X (MacDougall-Shackleton et al. 1999), both males and females present a volume increase in the striatum from sensory to sensorimotor phase, suggesting that the observed volume increase might not relate to vocal-motor plasticity. The large subdivisions of the zebra finch brain likely contain distinct functional domains that present no clearly defined cytoarchitectonic borders and can only be properly identified based on tract tracing studies or, upon stimulation, by *in vivo* functional imaging. For example, specific parts of the dorsal NCL connect in a topographical manner to the dorsal intermediate arcopallium, as well as to the $LMAN_{shell}$ (Bottjer et al. 2000), and may serve in active song evaluation during vocal learning (Mandelblat-Cerf et al. 2014). Further, Wild and Farabaugh showed structural connectivity between the specific parts of the NCL and the basorostral nucleus (Wild et al. 1996).

#### 4.3.2 Sensorimotor vs crystallization

After the sensorimotor phase, only more rostrally situated brain structures appeared to change in volume. These include the caudal mesopallium (CM) and hyperpallium. Interestingly, both areas do not show volume differences in the early stages of vocal learning, instead a clear volume decrease is present from the sensorimotor to the crystallization phase, and to a lesser extent towards 200 dph. The hyperpallium apicale contains the Wulst which processes sensory information, including visual and somatosensory stimuli (Wild et al. 2000), and connects to nuclei related to song control and auditory system (Wild et al. 1999).

### 4.4 Methodological considerations

Repeated exposure to anesthesia or repeated scanning has been found to impact normal brain development, especially at very young ages (Szulc et al. 2015). Likewise, early nutritional stress in juvenile zebra finches impairs proper song learning reflected in poorer copies of the tutor song (Brumm et al. 2009). To evaluate potential experiment-induced confounds on brain development, we quantified song performance in adulthood. Using song similarity to tutor song as a proxy for song learning proficiency, we observed similarity scores in similar ranges as observed by others (Supplementary Information SI-3).

Bird brains differ fundamentally from mammalian brains as cortical tissue is organized in nuclei instead of cortical layers. Consequently, generating tissue probability maps that grossly reflect grey matter, white matter or cerebrospinal fluid was a challenge. To improve the quality of the automated image-based tissue segmentation performed in the FAST tool of FSL (Zhang et al. 2001), we first created a population-based template using ANTs (Avants et al. 2008). The resulting tissue probability maps could be readily inserted in the existing SPM VBM pipeline (Ashburner 2007, Ashburner et al. 2012). The segment-based template datasets generated by DARTEL ($c_1$, $c_2$ and $c_3$) can be made available upon request and will enable future MRI studies in zebra finches to directly start with image segmentation in SPM after the SLR without having to create an additional population-based template in other software programs.

The white matter segment, i.e. $c_2$, first decreased in volume until 40 dph after which its volume consistently increased towards 200 dph. In most mammalian species, white matter volume appears to increase over time at a regionally-specific rate. Consequently, the initial dip in relative white matter volume observed in this study does not fully align with these descriptions. A potential reason for this early volume decline might be attributed to using relative instead of absolute volumes, i.e. expressing white matter volume proportional to total brain volume. For example, if the total brain volume increases at a faster pace than the white matter compartment, the latter might appear to decrease in volume. However, plotting the absolute tissue segment volume in function of age (Figure SI-3) illustrates that also the absolute volume of the c2 segment decreases towards 120 and 200 dph. An alternative explanation for this effect might be found in the drastic changes in intrinsic tissue properties that occur in early postnatal life (developmental specificities of T1-and T2-weighted contrasts are demonstrated by (Leppert et al. 2009) and reviewed by (Deoni 2010, Dubois et al. 2014)). Such changes in T1- and T2-relaxation times can significantly alter the MR image contrast and make that in early ages myelinated tissues appear less hypo-intense on T2-weighted images compared to later ages. These changes in image contrast might affect the accuracy of the spatial

transformation and, since tissue segment volumes are in part based on the latter, might affect the volume determination.

Lastly, we did not expect to find unilateral sex differences in brain structure, since the previous studies did not report sex differences in brain structure to be confined to or more expressed in one hemisphere (Nixdorf-Bergweiler 1996). Studies assessing hemispheric asymmetry in brain structure have led to inconsistent reports (Williams et al. 1992, Floody et al. 1997), and, in contrast to other songbird species, there is no strong dominance to either side of the zebra finch syrinx for song production (Goller et al. 2004). We therefore argue that unilateral clusters might arise because of the method or stringent statistical thresholds applied in this study.

# 5 Conclusions

In sum, the work presented here is –to our knowledge– the first longitudinal *in vivo* imaging study performed in juvenile songbirds. The main aim of the present study was to create spatio-temporal maps informing which brain areas change in volume between consecutive sub-phases of vocal learning in male and female zebra finch brains. The resulting statistical maps clearly indicate that most of the large brain subdivisions that embed the auditory and song control areas display volume changes early in development, between 20 and 65 dph. Whole brain volume mimics the inverted U-shape observed in humans. Further, the implemented data processing protocol appears sensitive enough to trace established volume differences between both sexes and led to the identification of previously unknown sex-differences in volume of the tOM and NIf. By uncovering novel sex differences and presenting volume changes that exclusively affect specific subparts of larger brain areas, this study clearly illustrates the advantage of brain-wide voxel-based research strategies that do not rely on *a priori* definition of brain regions-of-interest. Besides informing on general brain maturational processes in male and female zebra finches, and drawing interesting parallels to mammalian brain development, this work can serve as a reference for future neurodevelopmental imaging studies in zebra finches.

## Acknowledgements

We thank Prof Dr J.M. Wild for his insights and advice at localizing brain areas, and Prof. Dr. E. Fransen (StatUa Center for Statistics) for a critical revision of the statistical methodology (mixed models). The computational resources and services used in this work to build the population-based template (created using ANTs) were provided by the HPC core facility CalcUA of the Universiteit Antwerpen, the VSC (Flemish Supercomputer Center), funded by the Hercules Foundation and the Flemish Government – department EWI. This work was supported by grants from the Research

Foundation—Flanders (FWO, Project No. G030213N, G044311N and G037813N), the Hercules Foundation (Grant No. AUHA0012), and Interuniversity Attraction Poles (IAP) initiated by the Belgian Science Policy Office ('PLASTOSCINE': P7/17 and P7/11) to AVdL. JH is a PhD student supported by the University of Antwerp.

## References

Akutagawa, E. and M. Konishi (2010). "New brain pathways found in the vocal control system of a songbird." *The Journal of Comparative Neurology* 518(15): 3086-3100, 10.1002/cne.22383.

Ashburner, J. (2007). "A fast diffeomorphic image registration algorithm." *NeuroImage* 38(1): 95-113, http://dx.doi.org/10.1016/j.neuroimage.2007.07.007.

Ashburner, J. and K. J. Friston (2009). "Computing average shaped tissue probability templates." *NeuroImage* 45(2): 333-341, http://dx.doi.org/10.1016/j.neuroimage.2008.12.008.

Ashburner, J. and G. R. Ridgway (2012). "Symmetric Diffeomorphic Modeling of Longitudinal Structural MRI." *Frontiers in Neuroscience* 6: 197, 10.3389/fnins.2012.00197.

Ashburner, J. and G. R. Ridgway (2015). Tensor-Based Morphometry A2 - Toga, Arthur W. *Brain Mapping*. Waltham, Academic Press**:** 383-394.

Avants, B. B., C. L. Epstein, M. Grossman and J. C. Gee (2008). "Symmetric diffeomorphic image registration with cross-correlation: Evaluating automated labeling of elderly and neurodegenerative brain." *Medical Image Analysis* 12(1): 26-41, http://dx.doi.org/10.1016/j.media.2007.06.004.

Avants, B. B., N. J. Tustison, G. Song, P. A. Cook, A. Klein and J. C. Gee (2011). "A reproducible evaluation of ANTs similarity metric performance in brain image registration." *NeuroImage* 54(3): 2033-2044, https://doi.org/10.1016/j.neuroimage.2010.09.025.

Bischof, H.-J. and J. Niemann (1990). "Contralateral projections of the optic tectum in the zebra finch (Taenopygia guttata castanotis)." *Cell and Tissue Research* 262(2): 307-313, 10.1007/bf00309886.

Bolhuis, J. J., K. Okanoya and C. Scharff (2010). "Twitter evolution: converging mechanisms in birdsong and human speech." *Nat Rev Neurosci* 11(11): 747-759, http://www.nature.com/nrn/journal/v11/n11/suppinfo/nrn2931_S1.html.

Bottjer, S. W. and A. P. Arnold (1997). "DEVELOPMENTAL PLASTICITY IN NEURAL CIRCUITS FOR A LEARNED BEHAVIOR." *Annual Review of Neuroscience* 20(1): 459-481, 10.1146/annurev.neuro.20.1.459.

Bottjer, S. W., J. D. Brady and B. Cribbs (2000). "Connections of a motor cortical region in zebra finches: Relation to pathways for vocal learning." *The Journal of Comparative Neurology* 420(2): 244-260, 10.1002/(SICI)1096-9861(20000501)420:2<244::AID-CNE7>3.0.CO;2-M.

Brainard, M. S. (2004). "Contributions of the Anterior Forebrain Pathway to Vocal Plasticity." *Annals of the New York Academy of Sciences* 1016(1): 377-394, 10.1196/annals.1298.042.

Brainard, M. S. and A. J. Doupe (2000). "Interruption of a basal ganglia-forebrain circuit prevents plasticity of learned vocalizations." *Nature* 404(6779): 762-766,

Brainard, M. S. and A. J. Doupe (2013). "Translating Birdsong: Songbirds as a Model for Basic and Applied Medical Research." *Annual Review of Neuroscience* 36(1): 489-517, doi:10.1146/annurev-neuro-060909-152826.

Bredenkotter, M., J. Engelage and H.-J. Bischof (1996). "Visual system alterations in white zebra finches." *BRAIN BEHAVIOR AND EVOLUTION* 47(1),

Brumm, H., S. A. Zollinger and P. J. B. Slater (2009). "Developmental stress affects song learning but not song complexity and vocal amplitude in zebra finches." *Behavioral Ecology and Sociobiology* 63(9): 1387-1395, 10.1007/s00265-009-0749-y.

Calabrese, E., A. Badea, C. Watson and G. A. Johnson (2013). "A quantitative magnetic resonance histology atlas of postnatal rat brain development with regional estimates of growth and variability." *NeuroImage* 71: 196-206, http://dx.doi.org/10.1016/j.neuroimage.2013.01.017.

Calabrese, E. and G. A. Johnson (2013). "Diffusion tensor magnetic resonance histology reveals microstructural changes in the developing rat brain." *NeuroImage* 79(Supplement C): 329-339, https://doi.org/10.1016/j.neuroimage.2013.04.101.

Calabrese, E., G. A. Johnson and C. Watson (2013). "An ontology-based segmentation scheme for tracking postnatal changes in the developing rodent brain with MRI." *NeuroImage* 67: 375-384, http://dx.doi.org/10.1016/j.neuroimage.2012.11.037.

Cardin, J. A., J. N. Raksin and M. F. Schmidt (2005). "Sensorimotor Nucleus NIf Is Necessary for Auditory Processing But Not Vocal Motor Output in the Avian Song System." *Journal of Neurophysiology* 93(4): 2157-2166, 10.1152/jn.01001.2004.

Chuang, N., S. Mori, A. Yamamoto, H. Jiang, X. Ye, X. Xu, L. J. Richards, J. Nathans, M. I. Miller, A. W. Toga, R. L. Sidman and J. Zhang (2011). "An MRI-based atlas and database of the developing mouse brain." *NeuroImage* 54(1): 80-89, http://dx.doi.org/10.1016/j.neuroimage.2010.07.043.

Coleman, M. J., A. Roy, J. M. Wild and R. Mooney (2007). "Thalamic Gating of Auditory Responses in Telencephalic Song Control Nuclei." *The Journal of Neuroscience* 27(37): 10024-10036, 10.1523/jneurosci.2215-07.2007.

Deoni, S. C. L. (2010). "Quantitative Relaxometry of the Brain." *Topics in Magnetic Resonance Imaging* 21(2): 101-113 110.1097/RMR.1090b1013e31821e31856d31828,

Dubois, J., G. Dehaene-Lambertz, S. Kulikova, C. Poupon, P. S. Hüppi and L. Hertz-Pannier (2014). "The early development of brain white matter: A review of imaging studies in fetuses, newborns and infants." *Neuroscience* 276: 48-71, http://dx.doi.org/10.1016/j.neuroscience.2013.12.044.

Floody, O. R. and A. P. Arnold (1997). "Song Lateralization in the Zebra Finch." *Hormones and Behavior* 31(1): 25-34, http://dx.doi.org/10.1006/hbeh.1997.1368.

Giedd, J. N., J. Blumenthal, N. O. Jeffries, F. X. Castellanos, H. Liu, A. Zijdenbos, T. Paus, A. C. Evans and J. L. Rapoport (1999). "Brain development during childhood and adolescence: a longitudinal MRI study." *Nat Neurosci* 2(10): 861-863,

Giedd, J. N., A. Raznahan, A. Alexander-Bloch, E. Schmitt, N. Gogtay and J. L. Rapoport (2014). "Child Psychiatry Branch of the National Institute of Mental Health Longitudinal Structural Magnetic Resonance Imaging Study of Human Brain Development." *Neuropsychopharmacology* 40: 43, 10.1038/npp.2014.236.

Gogtay, N., J. N. Giedd, L. Lusk, K. M. Hayashi, D. Greenstein, A. C. Vaituzis, T. F. Nugent, D. H. Herman, L. S. Clasen, A. W. Toga, J. L. Rapoport and P. M. Thompson (2004). "Dynamic mapping of human cortical development during childhood through early adulthood." *Proceedings of the National Academy of Sciences of the United States of America* 101(21): 8174-8179, 10.1073/pnas.0402680101.

Goller, F. and B. G. Cooper (2004). "Peripheral Motor Dynamics of Song Production in the Zebra Finch." *Annals of the New York Academy of Sciences* 1016(1): 130-152, 10.1196/annals.1298.009.

Group., B. D. C. (2012). "Total and Regional Brain Volumes in a Population-Based Normative Sample from 4 to 18 Years: The NIH MRI Study of Normal Brain Development." *Cerebral Cortex* 22(1): 1-12, 10.1093/cercor/bhr018.

Hahnloser, R. H. R. and M. S. Fee (2007). "Sleep-Related Spike Bursts in HVC Are Driven by the Nucleus Interface of the Nidopallium." *Journal of Neurophysiology* 97(1): 423-435, 10.1152/jn.00547.2006.

Hammelrath, L., S. Škokić, A. Khmelinskii, A. Hess, N. van der Knaap, M. Staring, B. P. F. Lelieveldt, D. Wiedermann and M. Hoehn (2016). "Morphological maturation of the mouse brain: An in vivo MRI and histology investigation." *NeuroImage* 125: 144-152, http://dx.doi.org/10.1016/j.neuroimage.2015.10.009.

Holloway, C. C. and D. F. Clayton (2001). "Estrogen synthesis in the male brain triggers development of the avian song control pathway in vitro." *Nat Neurosci* 4(2): 170-175, http://www.nature.com/neuro/journal/v4/n2/suppinfo/nn0201_170_S1.html.

Immelmann, K. (1969). "{Song development in the zebra finch and other estrildid finches}." *Bird vocalizations (Hinde RA, ed)*: 61-74, citeulike-article-id:8343889.

Jenkinson, M., C. F. Beckmann, T. E. J. Behrens, M. W. Woolrich and S. M. Smith (2012). "FSL." *NeuroImage* 62(2): 782-790, http://dx.doi.org/10.1016/j.neuroimage.2011.09.015.

Karten, H. J., A. Brzozowska-Prechtl, P. V. Lovell, D. D. Tang, C. V. Mello, H. Wang and P. P. Mitra (2013). "Digital Atlas of the Zebra Finch (Taeniopygia guttata) Brain: a High Resolution Photo Atlas." *The Journal of comparative neurology* 521(16): 3702-3715, 10.1002/cne.23443.

Klein, A., J. Andersson, B. A. Ardekani, J. Ashburner, B. Avants, M.-C. Chiang, G. E. Christensen, D. L. Collins, J. Gee, P. Hellier, J. H. Song, M. Jenkinson, C. Lepage, D. Rueckert, P. Thompson, T. Vercauteren, R. P. Woods, J. J. Mann and R. V. Parsey (2009). "Evaluation of 14 nonlinear deformation algorithms applied to human brain MRI registration." *NeuroImage* 46(3): 786-802, https://doi.org/10.1016/j.neuroimage.2008.12.037.

Knudsen, E. I. (2004). "Sensitive Periods in the Development of the Brain and Behavior." *Journal of Cognitive Neuroscience* 16(8): 1412-1425, 10.1162/0898929042304796.

Konishi, M. and E. Akutagawa (1985). "Neuronal growth, atrophy and death in a sexually dimorphic song nucleus in the zebra finch brain." *Nature* 315(6015): 145-147,

Lebel, C., S. Treit and C. Beaulieu "A review of diffusion MRI of typical white matter development from early childhood to young adulthood." *NMR in Biomedicine*: e3778-n/a, 10.1002/nbm.3778.

Lenroot, R. K., N. Gogtay, D. K. Greenstein, E. M. Wells, G. L. Wallace, L. S. Clasen, J. D. Blumenthal, J. Lerch, A. P. Zijdenbos, A. C. Evans, P. M. Thompson and J. N. Giedd (2007). "Sexual dimorphism of brain developmental trajectories during childhood and adolescence." *NeuroImage* 36(4): 1065-1073, http://dx.doi.org/10.1016/j.neuroimage.2007.03.053.

Leppert, I. R., C. R. Almli, R. C. McKinstry, R. V. Mulkern, C. Pierpaoli, M. J. Rivkin and G. B. Pike (2009). "T2 relaxometry of normal pediatric brain development." *Journal of Magnetic Resonance Imaging* 29(2): 258-267, 10.1002/jmri.21646.

Lewandowski, B., A. Vyssotski, R. H. R. Hahnloser and M. Schmidt (2013). "At the interface of the auditory and vocal motor systems: NIf and its role in vocal processing, production and learning." *Journal of Physiology-Paris* 107(3): 178-192, https://doi.org/10.1016/j.jphysparis.2013.04.001.

Lewandowski, B. C. and M. Schmidt (2011). "Short Bouts of Vocalization Induce Long-Lasting Fast Gamma Oscillations in a Sensorimotor Nucleus." *The Journal of Neuroscience* 31(39): 13936-13948, 10.1523/jneurosci.6809-10.2011.

MacDougall-Shackleton, S. A. and G. F. Ball (1999). "Comparative studies of sex differences in the song-control system of songbirds." *Trends in Neurosciences* 22(10): 432-436, http://dx.doi.org/10.1016/S0166-2236(99)01434-4.

Mandelblat-Cerf, Y., L. Las, N. Denisenko and M. S. Fee (2014). "A role for descending auditory cortical projections in songbird vocal learning." *eLife* 3: e02152, 10.7554/eLife.02152.

Mello, C. V. and S. Ribeiro (1998). "ZENK protein regulation by song in the brain of songbirds." *The Journal of Comparative Neurology* 393(4): 426-438, 10.1002/(SICI)1096-9861(19980420)393:4<426::AID-CNE3>3.0.CO;2-2.

Mengler, L., A. Khmelinskii, M. Diedenhofen, C. Po, M. Staring, B. P. F. Lelieveldt and M. Hoehn (2014). "Brain maturation of the adolescent rat cortex and striatum: Changes in volume and myelination." *NeuroImage* 84: 35-44, http://dx.doi.org/10.1016/j.neuroimage.2013.08.034.

Mills, K. L. and C. K. Tamnes (2014). "Methods and considerations for longitudinal structural brain imaging analysis across development." *Developmental Cognitive Neuroscience* 9(0): 172-190, http://dx.doi.org/10.1016/j.dcn.2014.04.004.

Morita, T., M. Asada and E. Naito (2016). "Contribution of Neuroimaging Studies to Understanding Development of Human Cognitive Brain Functions." *Frontiers in Human Neuroscience* 10(464), 10.3389/fnhum.2016.00464.

Naie, K. and R. H. R. Hahnloser (2011). "Regulation of learned vocal behavior by an auditory motor cortical nucleus in juvenile zebra finches." *Journal of Neurophysiology* 106(1): 291-300, 10.1152/jn.01035.2010.

Nixdorf-Bergweiler, B. E. (1996). "Divergent and parallel development in volume sizes of telencephalic song nuclei in and female zebra finches." *The Journal of Comparative Neurology* 375(3): 445-456, 10.1002/(SICI)1096-9861(19961118)375:3<445::AID-CNE7>3.0.CO;2-2.

Nottebohm, F. (1980). Brain pathways for vocal learning in birds: a review of the first 10 years. *Progress in Psychobiology and Physiological Psychology*. J. M. Sprague and A. N. Epstein. New York, Academic Press. 9**:** 85-214.

Nottebohm, F. and A. Arnold (1976). "Sexual dimorphism in vocal control areas of the songbird brain." *Science* 194(4261): 211-213, 10.1126/science.959852.

Perkel, D. J. (2004). "Origin of the Anterior Forebrain Pathway." *Annals of the New York Academy of Sciences* 1016(1): 736-748, 10.1196/annals.1298.039.

Person, A. L., S. D. Gale, M. A. Farries and D. J. Perkel (2008). "Organization of the songbird basal ganglia, including area X." *The Journal of Comparative Neurology* 508(5): 840-866, 10.1002/cne.21699.

Rathjen, S., R. Engelmann, S. Struif, T. Kaulisch, D. Stiller and S. Löwel (2003). "The growth of cat cerebral cortex in postnatal life: a magnetic resonance imaging study." *European Journal of Neuroscience* 18(7): 1797-1806, 10.1046/j.1460-9568.2003.02909.x.

Raznahan, A., P. W. Shaw, J. P. Lerch, L. S. Clasen, D. Greenstein, R. Berman, J. Pipitone, M. M. Chakravarty and J. N. Giedd (2014). "Longitudinal four-dimensional mapping of subcortical anatomy in human development." *Proceedings of the National Academy of Sciences of the United States of America* 111(4): 1592-1597, 10.1073/pnas.1316911111.

Reiner, A., A. V. Laverghetta, C. A. Meade, S. L. Cuthbertson and S. W. Bottjer (2004). "An immunohistochemical and pathway tracing study of the striatopallidal organization of area X in the male zebra finch." *The Journal of Comparative Neurology* 469(2): 239-261, 10.1002/cne.11012.

Reiner, A., D. J. Perkel, C. V. Mello and E. D. Jarvis (2004). "Songbirds and the Revised Avian Brain Nomenclature." *Annals of the New York Academy of Sciences* 1016(1): 77-108, 10.1196/annals.1298.013.

Reuter, M., N. J. Schmansky, H. D. Rosas and B. Fischl (2012). "Within-subject template estimation for unbiased longitudinal image analysis." *Neuroimage* 61(4): 1402-1418, 10.1016/j.neuroimage.2012.02.084.

Roberts, T. F., S. M. H. Gobes, M. Murugan, B. P. Ölveczky and R. Mooney (2012). "Motor circuits are required to encode a sensory model for imitative learning." *Nature Neuroscience* 15: 1454, 10.1038/nn.3206

https://www.nature.com/articles/nn.3206#supplementary-information.

Simpson, H. and D. Vicario (1990). "Brain pathways for learned and unlearned vocalizations differ in zebra finches." *The Journal of Neuroscience* 10(5): 1541-1556,

Szulc, K. U., J. P. Lerch, B. J. Nieman, B. B. Bartelle, M. Friedel, G. A. Suero-Abreu, C. Watson, A. L. Joyner and D. H. Turnbull (2015). "4D MEMRI atlas of neonatal FVB/N mouse brain development." *NeuroImage* 118: 49-62, 10.1016/j.neuroimage.2015.05.029.

Tchernichovski, O., P. P. Mitra, T. Lints and F. Nottebohm (2001). "Dynamics of the Vocal Imitation Process: How a Zebra Finch Learns Its Song." *Science* 291(5513): 2564-2569, 10.1126/science.1058522.

Wild, J. M. (1995). "Convergence of somatosensory and auditory projections in the avian torus semicircularis, including the central auditory nucleus." *The Journal of Comparative Neurology* 358(4): 465-486, 10.1002/cne.903580402.

Wild, J. M. (1997). "Neural pathways for the control of birdsong production." *Journal of Neurobiology* 33(5): 653-670, 10.1002/(SICI)1097-4695(19971105)33:5<653::AID-NEU11>3.0.CO;2-A.

Wild, J. M. and S. M. Farabaugh (1996). "Organization of afferent and efferent projections of the nucleus basalis prosencephali in a passerine, Taeniopygia guttata." *The Journal of Comparative Neurology* 365(2): 306-328, 10.1002/(SICI)1096-9861(19960205)365:2<306::AID-CNE8>3.0.CO;2-9.

712 Wild, J. M. and M. N. Williams (1999). "Rostral wulst of passerine birds: II. Intratelencephalic
713 projections to nuclei associated with the auditory and song systems." *The Journal of Comparative*
714 *Neurology* 413(4): 520-534, 10.1002/(SICI)1096-9861(19991101)413:4<520::AID-CNE3>3.0.CO;2-B.
715 Wild, J. M. and M. N. Williams (2000). "Rostral Wulst in passerine birds. I. Origin, course, and
716 terminations of an avian pyramidal tract." *The Journal of Comparative Neurology* 416(4): 429-450,
717 10.1002/(SICI)1096-9861(20000124)416:4<429::AID-CNE2>3.0.CO;2-X.
718 Wild, M. J., H. J. Karten and B. J. Frost (1993). "Connections of the auditory forebrain in the pigeon
719 (columba livia)." *The Journal of Comparative Neurology* 337(1): 32-62, 10.1002/cne.903370103.
720 Williams, H., L. A. Crane, T. K. Hale, M. A. Esposito and F. Nottebohm (1992). "Right-side dominance
721 for song control in the zebra finch." *Journal of Neurobiology* 23(8): 1006-1020,
722 10.1002/neu.480230807.
723 Woolley, S. M. N. and J. H. Casseday (2005). "Processing of Modulated Sounds in the Zebra Finch
724 Auditory Midbrain: Responses to Noise, Frequency Sweeps, and Sinusoidal Amplitude Modulations."
725 *Journal of Neurophysiology* 94(2): 1143-1157, 10.1152/jn.01064.2004.
726 Woolley, S. M. N., P. R. Gill and F. E. Theunissen (2006). "Stimulus-Dependent Auditory Tuning
727 Results in Synchronous Population Coding of Vocalizations in the Songbird Midbrain." *The Journal of*
728 *Neuroscience* 26(9): 2499-2512, 10.1523/jneurosci.3731-05.2006.
729 Zhang, J., M. I. Miller, C. Plachez, L. J. Richards, P. Yarowsky, P. van Zijl and S. Mori (2005). "Mapping
730 postnatal mouse brain development with diffusion tensor microimaging." *NeuroImage* 26(4): 1042-
731 1051, http://dx.doi.org/10.1016/j.neuroimage.2005.03.009.
732 Zhang, Y., M. Brady and S. Smith (2001). "Segmentation of brain MR images through a hidden
733 Markov random field model and the expectation-maximization algorithm." *IEEE Transactions on*
734 *Medical Imaging* 20(1): 45-57, 10.1109/42.906424.
735 Ziegler, W. and H. Ackermann (2017). "Subcortical Contributions to Motor Speech: Phylogenetic,
736 Developmental, Clinical." *Trends in Neurosciences* 40(8): 458-468,
737 https://doi.org/10.1016/j.tins.2017.06.005.

## Inline supplementary information

**ISI-1: Sex differences in local tissue volume**

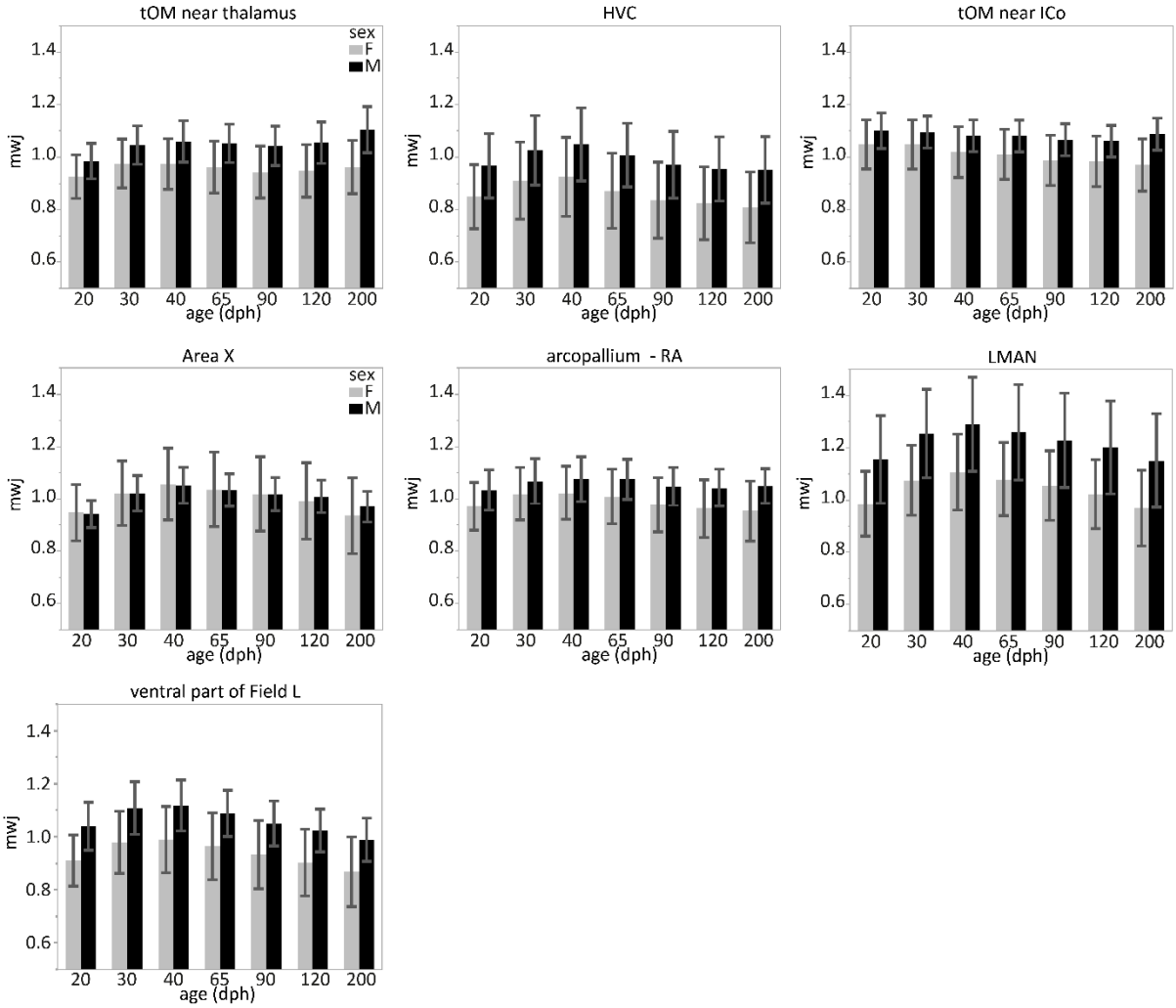


**Figure ISI-1: Bar graphs link sex differences detected in the modulated jacobian determinants.** The graphs include the modulated jacobian determinant (mwj) of the cluster-based ROIs which are based on the statistical maps of the voxel-wise ANOVA's on the modulated jacobian determinant maps. The jacobian determinants are plotted as mean ± standard deviation.

**ISI-2: Bird brain anatomy**

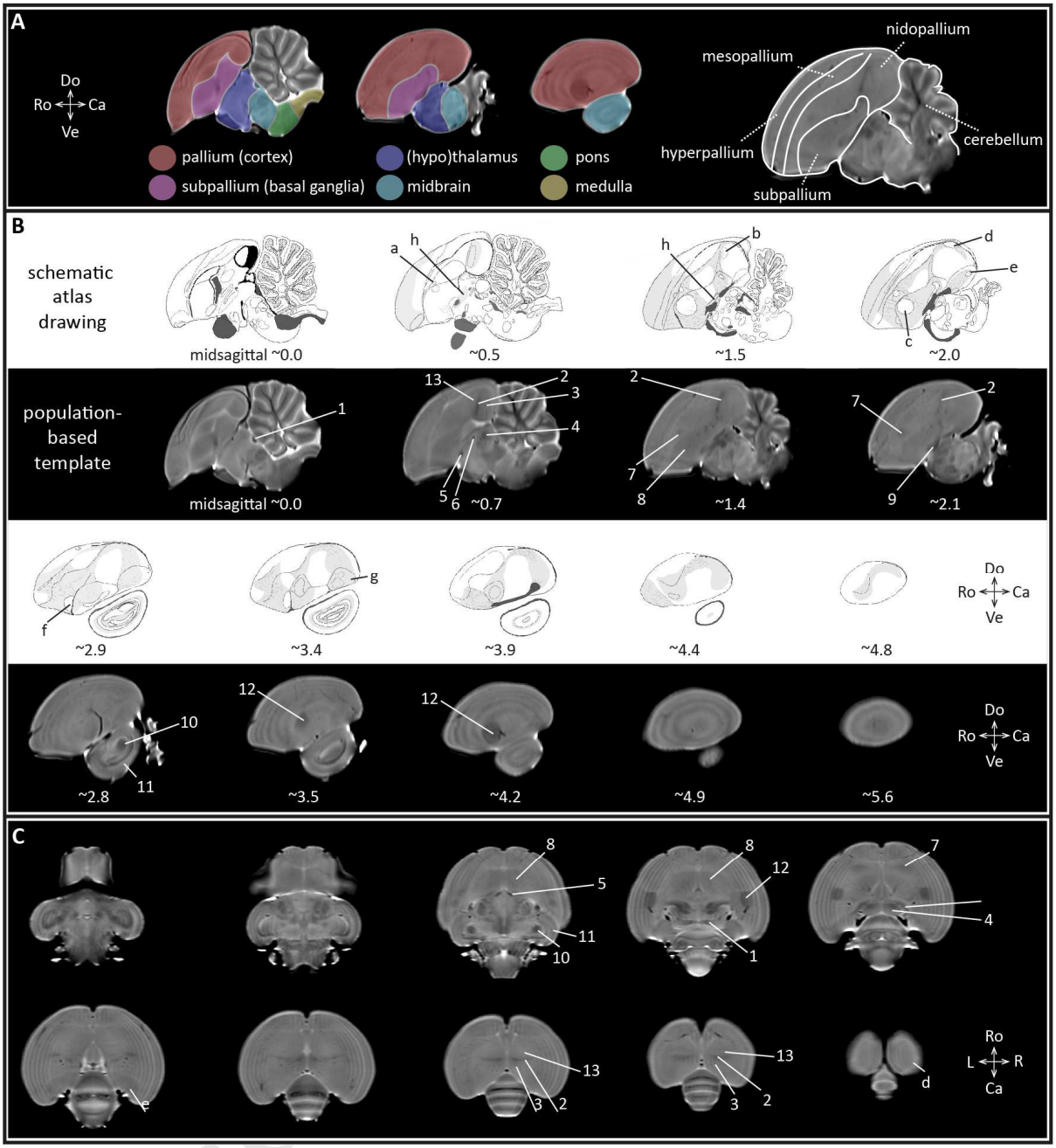


**Figure ISI-2: Bird brain anatomy**. **A** informs on the different subdivisions of the zebra finch brain projected on the population-based template. The colors refer to pallium, subpallium, thalamus and hypothalamus, midbrain, pons and medulla. The drawing on the right subdivides the telencephalon in its different sub-regions delineated by laminae, and cerebellum. **B** illustrates sagittal slices of the bird brain including schematic atlas drawings obtained from the zebra finch histological atlas browser (Oregon Health & Science University, Portland, OR 97239; http://www.zebrafinchatlas.org (Karten et al. 2013), and MR-images extracted from the population-based template. The numbers below the sagittal slices appoint the approximate (~) distance (mm) from the midline. Anatomical areas visible on the $T_2$-weighted MRI slices are appointed by numbers, while the letters indicate regions that are only visible on the schematic atlas drawings. **C** provides an overview of (the approximate position of) anatomical regions defined in (A) on horizontal slices derived from the population-based template. The numbers below the sagittal slices correspond to the approximate position (in 'mm' from the midline). Legend: a: MMAN; b: Field L2b; c: Area X; d: HVC; e: RA; f:

basorostral nucleus; g: lateral arcopallium; h: basal nucleus of Meynert and ventral pallidum; 1: posterior commissure; 2: Field L; 3: NCM; 4: thalamic zone; 5: TSM; 6: anterior commissure; 7: LMAN; 8: striatum including Area X; 9: FPL (lateral prosencephalic fascicle); 10: MLd; 11: TeO or ventral part of the optical lobe; 12: entopallium; 13: medial and lateral portion of the caudal mesopallium (respectively CMM and CML). Abbreviations: Do: dorsal; Ve: ventral; Ro; rostral: Ca: caudal; L: left; R: right.

## Data statement

The tissue segments can be made available upon request to the corresponding author.